Crystal structure and thermoelectric properties of the type-I clathrate compound Ba$_8$Ge$_{43}$ with an ordered arrangement of Ge vacancies

Norihiko L. Okamoto,[a)] Min Wook Oh, Takumi Nishii, Katsushi Tanaka, and Haruyuki Inui
Department of Materials Science and Engineering, Kyoto University Sakyo-ku, Kyoto 606-8501, Japan

The crystal structure of the type-I clathrate compound Ba$_8$Ge$_{43}$ has been investigated by x-ray diffraction and transmission electron microscopy. The thermoelectric properties of Ba$_8$Ge$_{43}$ have also been investigated. The crystal structure of Ba$_8$Ge$_{43}$ is different from that reported for the usual type-I clathrate compounds with the space group of $Pm\bar{3}n$ but is a superlattice structure based on the usual type-I clathrate structure due to the ordering of Ge vacancies in half the 6c sites of the usual type-I clathrate structure. The crystal structure of Ba$_8$Ge$_{43}$ belongs to the space group of $Ia\bar{3}d$ and Ge vacancies exclusively occupy the 24c sites. The thermoelectric properties of Ba$_8$Ge$_{43}$ are not particularly good, as exemplified by the rather low ZT value of 0.057 because of the high value of electrical resistivity, which may arise from the existence of Ge vacancies. © *2006 American Institute of Physics.* [DOI: 10.1063/1.2169869]

I. INTRODUCTION

Intermetallic clathrate compounds possess polyhedral cages encapsulating guest atoms.[1] The guest atoms are typically alkali metals or alkali-earth metals, whereas the cages consist of group-IV elements, Si, Ge, or Sn, although Al, Ga, In, As, or Sb can also be substituted for these elements to some extent. Clathrate compounds form in a variety of structure types, depending on the combination of different cages: pentagonal dodecahedra, tetrakaidecahedra, and hexakaidecahedra formed by 12 pentagonal faces, 12 pentagonal and 2 hexagonal faces, and 12 pentagonal and 4 hexagonal faces, respectively.[2–9] Three different types of intermetallic clathrate compounds, types I, II, and III, have been the subjects of extensive studies in the past for their crystal structures and physical properties.[2–9] The type-I structure comprises a cage structure consisting of two pentagonal dodecahedra and six tetrakaidecahedra and the corresponding unit cell is cubic with the space group of $Pm\bar{3}n$.[10] The type-II structure comprises a cage structure consisting of 16 pentagonal dodecahedra and 8 hexakaidecahedra. Its unit cell is also cubic with the space group of $Fd\bar{3}m$. On the other hand, the type-III structure comprises a cage structure consisting of eight dodecahedra only, belonging to the chiral space group of $P4_332$ or $P4_132$.

In recent years, intermetallic clathrate compounds, in particular, those of the type I have been investigated in a great endeavor in hopes of producing more efficient thermoelectric devices.[6,11] This is because intermetallic clathrate compounds generally show low thermal conductivity and reasonably high electrical conductivity, as explained with the concept of phonon glass, electron crystal (PGEC) by Slack.[12] The amorphouslike low thermal conductivity is believed to result from the "rattling" of the guest atoms in the polyhedral cages, which scatters heat-carrying phonons. On the other hand, the crystal-like high electrical conductivity is believed to be due to the high electrical conductivity of the cage structure itself in the absence of strong bonding with the guest atoms. The thermoelectric performance of intermetallic clathrate compounds is thus expected to be good, since the thermoelectric performance of a given material is evaluated with the dimensionless figure of merit, ZT$=\alpha^2 T/(\rho\lambda)$, where α, ρ, λ, and T stand for Seebeck coefficient, electrical resistivity, thermal conductivity, and temperature, respectively. Among the various types of clathrate compounds, some Ga-bearing type-I clathrate compounds, such as Sr$_8$Ga$_{16}$Ge$_{30}$,[13] have attracted considerable attention in recent years as thermoelectric materials of high performance because of their high values of Seebeck coefficient, in addition to the low thermal conductivity and relatively low electrical resistivity.

Type-I intermetallic clathrate compounds usually possess the general formula of M_8X_{46}, where M stands for K, Sr, or Ba while X for Si, Ge, or Sn. The usual type-I clathrate compounds consist of two pentagonal dodecahedra (X_{20}) and six tetrakaidecahedra (X_{24}) in the cubic unit cell of the space group of $Pm\bar{3}n$, as shown in Fig. 1. The X_{20} cages are located at the body center and all the corners of the cubic unit cell, while the X_{24} cages occupy the positions of linear-chain atoms of the A15 structure on the cube faces. The guest atoms (M) are located at the center of these cages. These two different types of cages (X_{20} and X_{24}) are connected with each other by sharing their pentagonal faces. X atoms constituting the cage structure are reported to occupy 6c, 16i, and 24k crystallographic sites in the space group of $Pm\bar{3}n$.[2] Of these three sites, 6c sites are repeatedly reported to be those preferentially occupied by substitutional atoms, as in the case of Sr$_8$Ga$_{16}$Ge$_{30}$.[14] Thus, the occupancy behavior of the 6c sites seems to play a very important role in determining the physical properties of type-I clathrate compounds. Some type-I clathrate compounds have been reported to have a chemical composition deviated from that expected from the formula of M_8X_{46}. These include Ba$_8$Ge$_{43}$,[15] K$_8$Ge$_{44}$,[16,17]

a)Electronic mail: nlokamoto@materials.mbox.media.kyoto-u.ac.jp
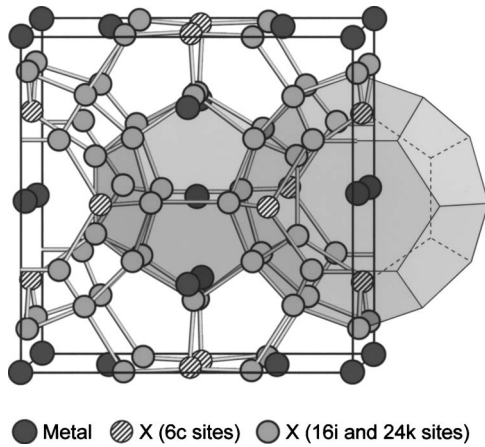
● Metal ▨ X (6c sites) ◯ X (16i and 24k sites)

FIG. 1. Crystal structure of type-I clathrate compounds. A dodecahedron (X_{20}) centered at the body center of the unit cell and one of its neighboring tetrakaidekahedra (X_{24}) are indicated in the figure. The atoms in the $6c$ sites are indicated with shaded circles.

$(K,Cs)_8Sn_{44}$, and Rb_8Sn_{44}.[8] One-third of the $6c$ sites for X atoms are reported to be randomly occupied by vacancies for K_8Ge_{44}, $(K,Cs)_8Sn_{44}$, and Rb_8Sn_{44} while Herrmann *et al.* inferred that half the $6c$ sites for Ge atoms are occupied by vacancies in an ordered manner in Ba_8Ge_{43}.[15] The clathrate type-I compound in the binary Ba–Ge system is confirmed to be stable only at the composition of Ba_8Ge_{43} from the study of the phase diagram reported by Cabrera *et al.*.[18] Although Herrmann *et al.* described the existence of additional reflections which they ascribed to the ordering of Ge vacancies in the $6c$ sites,[15] they did not determine the crystal structure of Ba_8Ge_{43}, i.e., how the ordering of Ge vacancies occurs in the crystal structure.

In the present study, we investigate the crystal structure of Ba_8Ge_{43} by x-ray diffraction and transmission electron microscopy (TEM), paying special attention to the identification of the possible ordering of Ge vacancies in the $6c$ sites. We also investigate thermoelectric properties of Ba_8Ge_{43} as a function of temperature. Implications of the ordering of Ge vacancies in the $6c$ sites will be briefly made on the thermoelectric properties of Ba_8Ge_{43}.

II. EXPERIMENTAL PROCEDURES

Specimens with the nominal composition of Ba_8Ge_{43} were prepared by Ar arc melting. After arc melting, the specimens were annealed at 790 °C in vacuum for 12 h followed by oil quenching. The annealed microstructures were examined by transmission electron microscopy. Thin foils for TEM observations were prepared by ion milling with 4 keV Ar ions. Calculations of electron-diffraction patterns and high-resolution TEM (HRTEM) images were made with the MAC TEMPAS software. The crystal structure was also analyzed by x-ray powder diffraction (with Mo $K\alpha$ radiation at 50 kV and 20 mA) and refined by the Rietveld method with the RIETAN-2000 program.[19] Measurements for Seebeck coefficient and electrical resistivity were made with our ZEM-2 apparatus (ULVAC, Japan) while measurements for thermal diffusivity and specific heat were made by the laser flash method.

III. RESULTS

A. Structural analysis

Specimens of the Ba_8Ge_{43} single phase can be obtained by oil-quenching above 770 °C. Otherwise, specimens exhibit the two-phase microstructure consisting of the $Ba_{24}Ge_{100}$ and Ge phases. This is consistent with the Ba–Ge phase diagram reported by Cabrera *et al.*,[18] in which the Ba_8Ge_{43} phase is indicated to be unstable below 770 °C and to decompose into the $Ba_{24}Ge_{100}$ and Ge phases below the temperature.

Selected area electron-diffraction (SAED) patterns of Ba_8Ge_{43} taken along various zone-axis orientations from the oil-quenched specimen are shown in Figs. 2(a)–2(d). SAED patterns of the corresponding zone-axis orientations calculated assuming the space group of $Pm\bar{3}n$ as the usual type-I clathrate compounds are shown in Figs. 2(e)–2(h). In the model structure based on the space group of $Pm\bar{3}n$, Ge vacancies are assumed to randomly distribute in $6c$ sites. Reflections of the 001 type in Fig. 2(e) are forbidden reflections that appear as "double" reflections, as is evident from the fact that they are extinct in Fig. 2(f). Many additional diffraction spots are observed in Figs. 2(b)–2(d) when compared to the corresponding calculated ones, as indicated by arrows. These additional diffraction spots are located at positions expressed with half-integer indices when indexed on the basis of the space group of $Pm\bar{3}n$. For example,
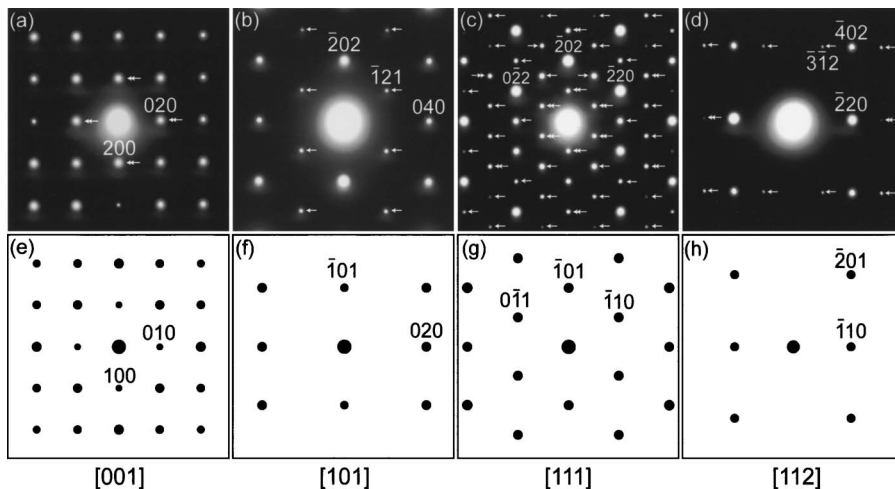

FIG. 2. SAED patterns of Ba_8Ge_{43} taken along [001], [101], [111], and [112] directions. The upper row [(a)–(d)] corresponds to experimental patterns, while the lower row [(e)–(h)] corresponds to calculated ones on the assumption that Ge vacancies in $6c$ sites are randomly distributed so as to maintain the space group of $Pm\bar{3}n$. Reflections indicated by arrows and double arrows in (a)–(d) are, respectively, superlattice reflections and forbidden reflections that appear as "double" reflections.
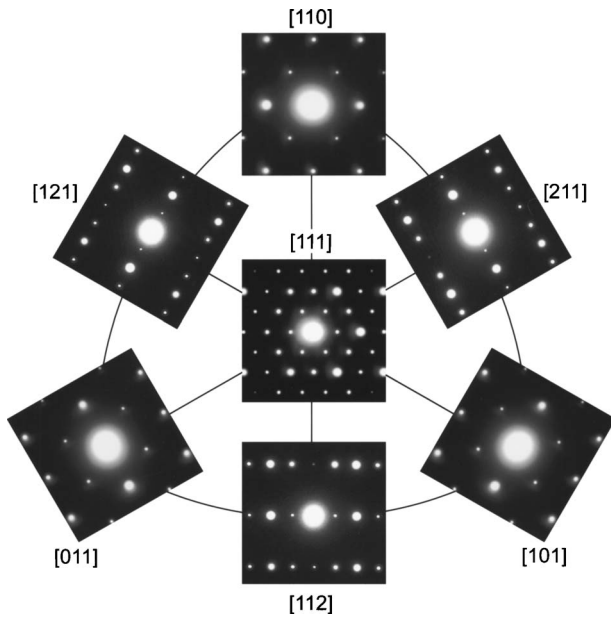
FIG. 3. SAED patterns of Ba_8Ge_{43} taken by tilting the thin foil specimen from [111] to $\langle 110 \rangle$- and $\langle 112 \rangle$-type zone-axis orientations, showing the threefold symmetry of the [111] direction.

$(\bar{1}/2, 1, 1/2)$-type reflections in the SAED's with the [101] and [111] incidence. This indicates that the Ge vacancies are ordered so that the unit cell of Ba_8Ge_{43} is larger than that of the usual type-I clathrate compounds with the space group of $Pm\bar{3}n$ by a factor of multiples of 2.

In order to determine the crystal system of Ba_8Ge_{43}, SAED patterns were taken by tilting the specimen from [111] to various zone-axis orientations, as shown in Fig. 3. All the SAED patterns with the incident beam parallel to $\langle 110 \rangle$-type zone-axis orientations are identical with each other and this is also the case for all the SAED patterns with the incident beam parallel to $\langle 112 \rangle$-type zone-axis orientations. This clearly indicates that [111] corresponds to the threefold axis and the crystal system is cubic. Thus, the unit cell of Ba_8Ge_{43} is cubic with the lattice parameter larger than that for the usual type-I clathrate compounds by a factor of multiples of 2.

The possible space groups for Ba_8Ge_{43} can be considered from the group theory by taking into account of k subgroups, in which some of translation symmetry elements are removed from the parent space group, and t subgroups, in

which some of rotation, glide, screw, reflection symmetry elements are removed from the parent space group. Since Ba_8Ge_{43} has a superlattice structure with a doubled lattice parameter due to the ordering of Ge vacancies in $6c$ sites, it loses translation symmetry of the space group of $Pm\bar{3}n$. This indicates that the k subgroups of $Pm\bar{3}n$ can be the space group of Ba_8Ge_{43}. There exist two such k subgroups; $Ia\bar{3}d$ and $Pm\bar{3}n$ with a lattice parameter doubled and tripled, respectively, as shown in the group-subgroup relation for the parent space group of $Pm\bar{3}n$ in Fig. 4. Since the lattice parameter of Ba_8Ge_{43} is larger than that for the parent unit cell by a factor of multiples of 2, $Pm\bar{3}n$ with a tripled lattice parameter is ruled out. Thus, the space group of $Ia\bar{3}d$ is one of the possible space groups for Ba_8Ge_{43}. The t subgroups of $Ia\bar{3}d$ can also be the possible space groups. These include $I\bar{4}3d$, $I4_132$, $Ia\bar{3}$, $R\bar{3}c$, and $I4_{1/a}cd$. The former three are of the cubic system while the last two are not. Since our TEM observations indicate that the crystal system of Ba_8Ge_{43} is cubic (Fig. 3), the last two t subgroups are ruled out. The t subgroups of the three t subgroups, $I\bar{4}3d$, $I4_132$, and $Ia\bar{3}$, can also be the possible space groups. These include $I2_13$, $R3c$, $I\bar{4}2d$, $R32$, $I4_122$, $R\bar{3}$, and $Ibca$ (Fig. 4). Of these seven space groups, only $I2_13$ is a cubic system and the other six are noncubic to be ruled out. The space group of $I2_13$ also has t subgroups of $R3$ and $I2_12_12_1$ as the possible space groups for Ba_8Ge_{43} but both of them are noncubic to be ruled out. Thus, the five cubic space groups of $Ia\bar{3}d$, $I\bar{4}3d$, $I4_132$, $Ia\bar{3}$, and $I2_13$ are the possible space groups for Ba_8Ge_{43} to be considered further.

We select the most plausible one from the five possible space groups by referring to the extinction rule. Indices for reflections expected to occur from the five possible space groups are tabulated in Table I together with those for reflections experimentally observed in the SAED patterns [Figs. 2(a)–2(d)]. The indices for experimentally observed reflections with asterisk (*) in Table I indicate that they are forbidden reflections that appear as double reflections in the SAED patterns, as indicated by double arrows in Figs. 2(a)–2(d). As seen in Table I, the extinction rule of the space group of $Ia\bar{3}d$ can only reproduce the observed SAED patterns. The space group of $Ia\bar{3}d$ is thus selected uniquely as the most plausible space group for Ba_8Ge_{43}.
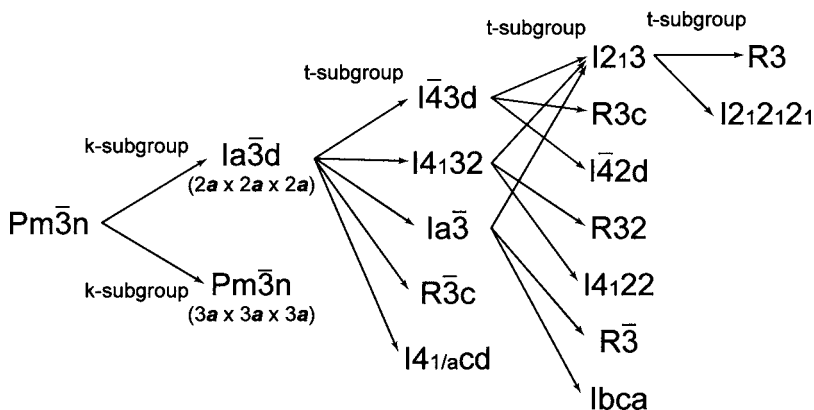

FIG. 4. Group-subgroup relation for the parent space group of $Pm\bar{3}n$.

TABLE I. Indices of observed reflections in the SAED patterns [Figs. 2(a)–2(d)] and those of possible reflections for the five structure models with the space group of $Ia\bar{3}d$, $I\bar{4}3d$, $I4_132$, $Ia\bar{3}$, and $I2_13$.

	Space group				
Experiment	$Ia\bar{3}d$	$I\bar{4}3d$	$I4_132$	$Ia\bar{3}$	$I2_13$
110*			110		110
200*				200	200
211	211	211	211	211	211
220	220	220	220	220	220
		310	310		310
			222	222	222
321	321	321	321	321	321
400	400	400	400	400	400
			411	411	411
330*			330		330
420	420	420	420	420	420
332	332	332	332	332	332
422	422	422	422	422	422
		510	510		510
431	431	431	431	431	431
521	521	521	521	521	521

FIG. 5. Possible vacancy positions on the planes of $x=0$ and $1/2$ in the superlattice unit cell with the space group of $Ia\bar{3}d$.

Vacancies have frequently been claimed to occupy the $6c$ sites in many of usual type-I clathrate compounds with the space group of $Pm\bar{3}n$.[8,15–17] The $6c$ sites of the parent space group of $Pm\bar{3}n$ correspond to the $24c$ and $24d$ sites of the space group of $Ia\bar{3}d$, as shown in Fig. 5. Two different models can be considered for the crystal structure of Ba_8Ge_{43}, depending on whether vacancies are exclusively in $24c$ sites or in $24d$ sites. However, it was impossible to distinguish one model from the other by x-ray powder diffraction, because of the weak intensity for superlattice reflections and the very small difference in their structure factors. We thus employ HRTEM in order to determine Ge vacancy sites in Ba_8Ge_{43}. HRTEM images of Ba_8Ge_{43} taken along the [111] direction with five different defocus values are shown in Figs. 6(a)–6(e). The corresponding calculated images are shown in Figs. 6(f)–6(j) for the model with Ge vacancies in the $24c$ sites and in Figs. 6(k)–6(o) for the model with Ge vacancies in the $24d$ sites. In the calculation, the accelerating voltage of 350 kV, the crystal thickness of 42 nm, and defocus values indicated at the top of the images are assumed
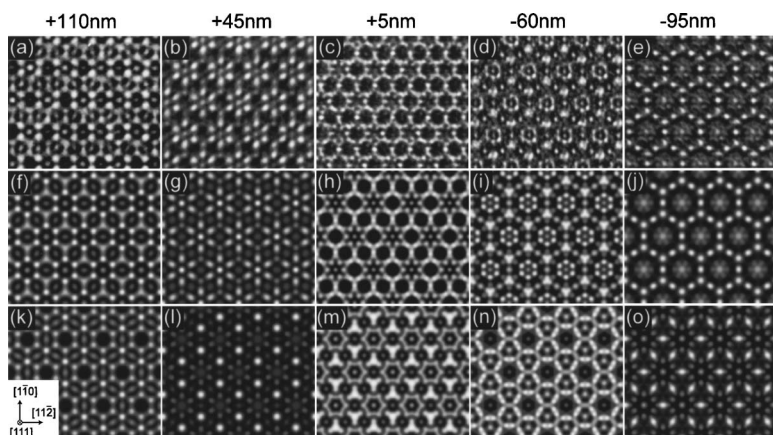
with the crystallographic parameters obtained for each of the models from the Rietveld refinement. As seen in Fig. 6, the experimental HRTEM images are better reproduced with the model of Ge vacancies in the $24c$ sites. Ge vacancies are thus determined to be exclusively in the $24c$ sites of the the space group of $Ia\bar{3}d$. It is rather surprising to notice that the two models with different distributions of Ge vacancies, which cannot be distinguished by x-ray diffraction, can be distinguished from each other by HRTEM. This is actually due to the fact that the vacancy distribution for the one model is quite different from that for the other in the [111] projections, as shown in Fig. 7.

We thus determine that the crystal structure of Ba_8Ge_{43} belongs to the cubic space group of $Ia\bar{3}d$ and is a superlattice structure based on the structure of usual type-I clathrate compounds with the doubled lattice parameter. The doubling of the unit cell is due to the ordering of Ge vacancies in the $24c$ site. The crystal structure can be thought of as being made up of eight unit cells of usual type-I clathrate compounds with four different Ge vacancy distributions [A–D in Fig. 8(a)] so that the lattice parameter of the unit cell is doubled [Fig. 8(b)].

Because the crystal structure of Ba_8Ge_{43} is a superlattice structure based on the usual type-I clathrate compounds [Fig. 8(b)], antiphase boundaries (APB's) are observed to usually form in the microstructure, as shown in the dark-field image of Fig. 9(a) formed with a 112-type superlattice reflection. These APB's are observed not to lie on any particular crystallographic planes, indicating they are of thermal origin. In fact, the domain size bounded by APB's increases as the

FIG. 6. Experimental HRTEM images of Ba_8Ge_{43} taken along the [111] direction with five different defocus values [(a)–(e)]. Corresponding HRTEM images calculated for the structure models with Ge vacancies in $24c$ sites [(f)–(j)] and in $24d$ sites [(k)–(o)].
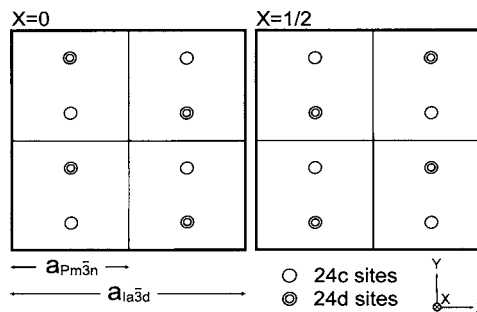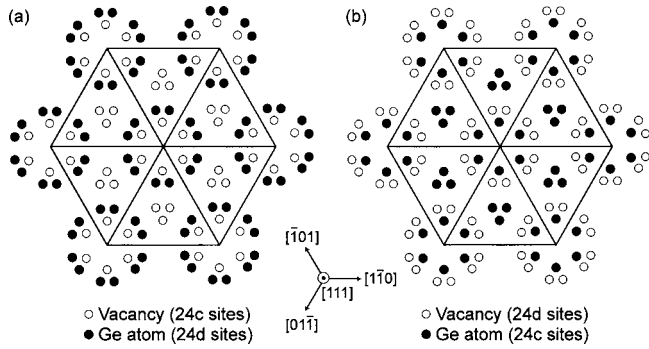
FIG. 7. [111] projection of 24c and 24d sites; (a) and (b) are for models with Ge vacancies in 24c sites and 24d sites, respectively.

aging time at 790 °C prior to quenching is increased. A HR-TEM image from the same crystal of Fig. 9(a) taken along the [111] direction is shown in Fig. 9(b), revealing an inclined APB (as outlined) across which the image contrast is shifted by a vector of the $1/6\langle 112 \rangle$ type in the projection. The shift by a vector of the $1/6\langle 112 \rangle$ type in the $\langle 111 \rangle$ projection corresponds to the displacement vectors of the $1/2\langle 110 \rangle$ and $1/2\langle 001 \rangle$ types for the APB's. These two vectors are equivalent to each other since these two differ from each other by a vector of the $1/2\langle 111 \rangle$ type, which is a translation vector of the corresponding superlattice.

B. Transport properties

Values of electrical resistivity, Seebeck coefficient, and thermal conductivity of Ba$_8$Ge$_{43}$ are shown respectively in
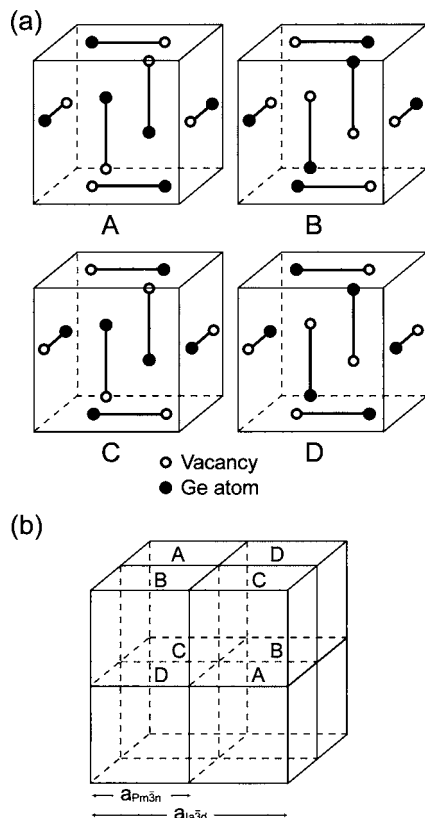

FIG. 8. (a) Four different subunit cells with different distributions of Ge vacancies in 6c sites of the usual type-I clathrate compound. (b) Unit cell of Ba$_8$Ge$_{43}$ corresponding to a superlattice formed by stacking eight subunit cells shown in (a).
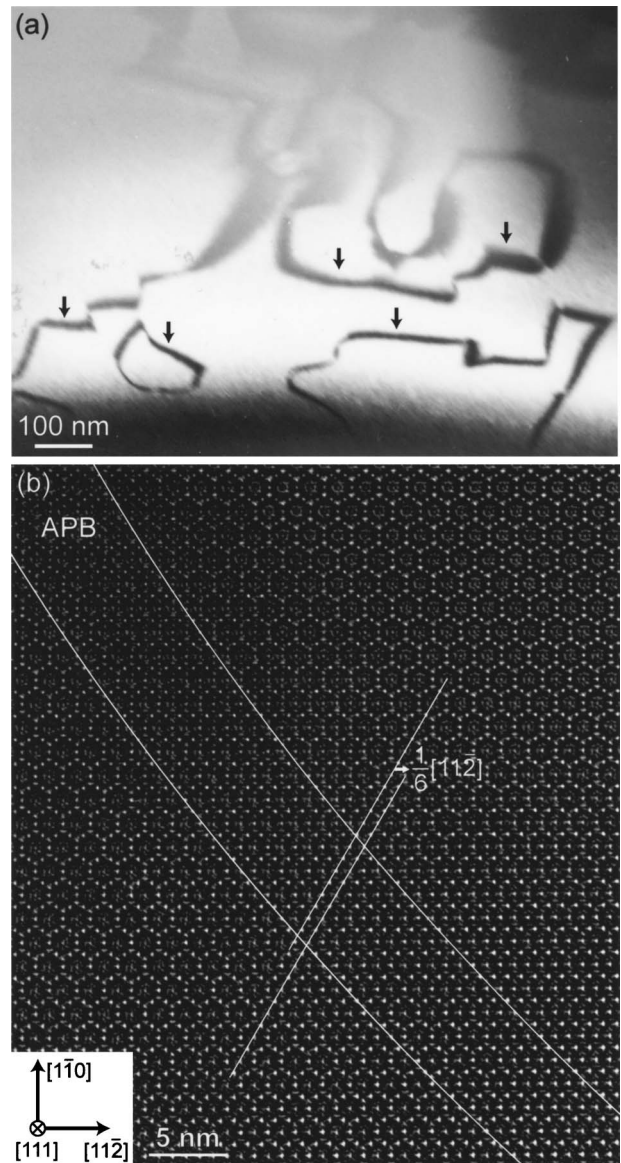

FIG. 9. APB's observed in Ba$_8$Ge$_{43}$ quenched from 790 °C: (a) dark-field image formed with a 112-type superlattice reflection and (b) HRTEM image taken along [111].

Figs. 10(a)–10(c) as a function of temperature. The value of electrical resistivity is as high as about 10^{-3} Ω m at room temperature and it decreases with the increase in temperature up to 400 °C on heating, which is a characteristic of semiconductor, followed by a sudden increase between 400 and 500 °C and then by a decrease again above 500 °C. On the other hand, the value of electrical resistivity is almost independent of temperature on cooling from 700 °C. The value of Seebeck coefficient is always negative, as in other type-I clathrate compounds[11,13] and the absolute value increases with the increase in temperature up to 400 °C, followed by a sharp increase by 200 μV/K at about 500 °C and then by a sharp decrease up to 600 °C. On cooling from 700 °C, the absolute value of Seebeck coefficient decreases as the temperature is decreased. The sharp change in values of electrical resistivity and Seebeck coefficient on heating above 400 °C is due to the phase decomposition of Ba$_8$Ge$_{43}$ into Ba$_{24}$Ge$_{100}$ and Ge phases. In fact, scanning electron micros-
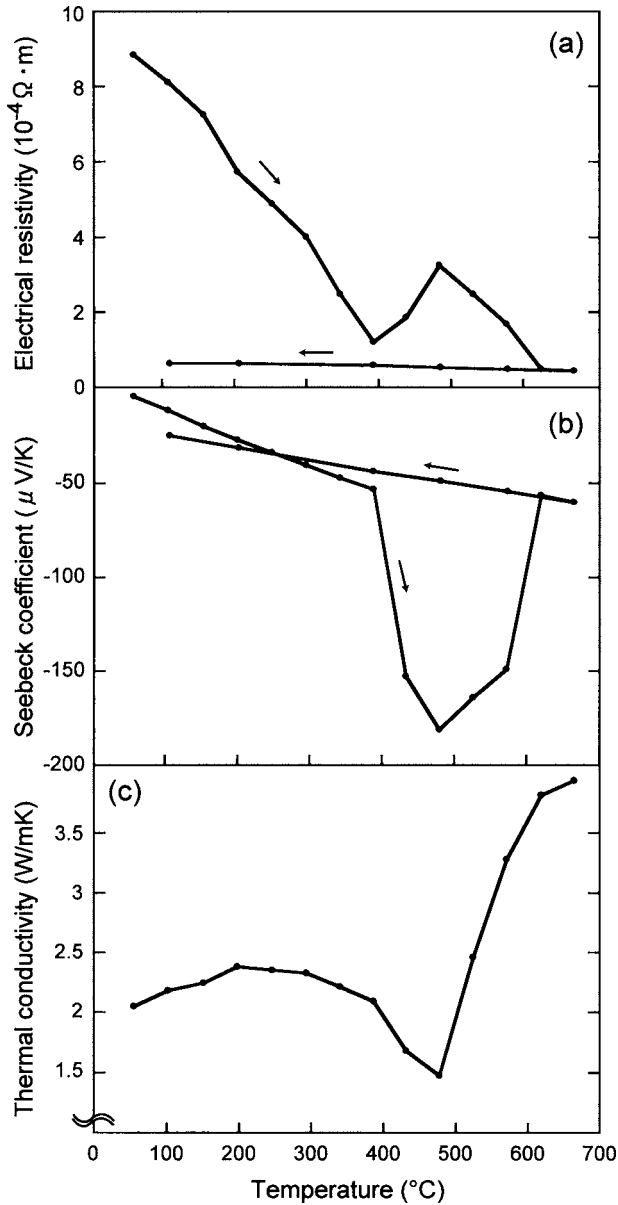
FIG. 10. (a) Electrical resistivity, (b) Seebeck coefficient, and (c) thermal conductivity of Ba_8Ge_{43} plotted as a function of temperature.

FIG. 11. SEM backscattered electron image of the specimen after the measurement, indicating the phase decomposition of Ba_8Ge_{43} into $Ba_{24}Ge_{100}$ (gray) and Ge (black) phases.

thermal conductivity below 400 °C is larger than those reported for other type-I clathrate compounds such as $Sr_8Ga_{16}Ge_{30}$.[13]

Values of the dimensionless figure of merit ZT calculated with the physical parameters of Fig. 10 are plotted in Fig. 12 as a function of temperature. The value of ZT increases as the temperature is increased to 0.057 at 420 °C, followed by a decrease with the increase in temperature above that temperature. The ZT value is considerably small in the whole temperature range because of the high electrical resistivity and low Seebeck coefficient.

IV. DISCUSSION

Our analysis has indicated that the crystal structure of Ba_8Ge_{43} is different from that reported for the usual type-I clathrate compounds with the space group of $Pm\bar{3}n$ but is a superlattice structure based on the usual type-I clathrate structure with the doubled lattice parameter, belonging to the space group of $Ia\bar{3}d$. Ge vacancies in half the $6c$ sites of the usual type-I clathrate structure are distributed in an ordered manner so as to form the superlattice structure. HRTEM imaging clearly indicates that Ge vacancies are exclusively in the $24c$ sites. In view of the weakness of intensities for superlattice reflections, crystal structure refinement to deduce

copy (SEM) observations of the specimen after the measurement have revealed the phase decomposition, as shown in Fig. 11. The value of electrical resistivity of Ba_8Ge_{43} is larger than that reported for $Sr_8Ga_{16}Ge_{30}$, which is free from Ge vacancies, by an order of magnitude.[13] The cagelike framework consisting of Ge atoms in the clathrate compounds is considered to play an important role in electrical conduction. Since the $6c$ sites of the usual type-I clathrate compounds correspond to the linkage points of four Ge_{24} cages, vacancies located there are considered to increase the value of electrical resistivity of Ba_8Ge_{43}. The value of thermal conductivity for Ba_8Ge_{43} shows a decrease with the increase in temperature from 200 °C, followed by a sharp increase above 500 °C. The sharp increase in thermal conductivity above 500 °C is also due to the phase decomposition of Ba_8Ge_{43} into $Ba_{24}Ge_{100}$ and Ge phases. The high value of thermal conductivity at high temperatures may be due to the high thermal conductivity of the Ge phase.[20] The value of
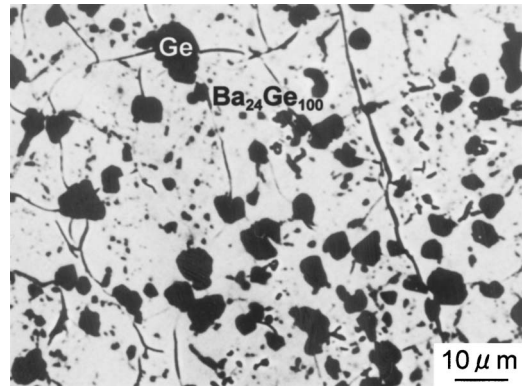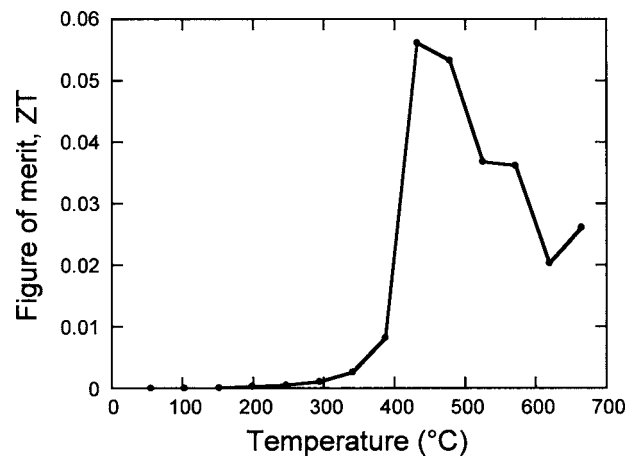

FIG. 12. Dimensionless figure of merit ZT of Ba_8Ge_{43} plotted as a function of temperature.

atomic coordinates, thermal factors, and so on for Ba_8Ge_{43} may not be easily made by x-ray diffraction with a conventional x-ray source such as that used in the present study. Structure refinement of Ba_8Ge_{43} by x-ray diffraction with synchrotron radiation is under way in our group.

One-third of the 6c sites for X atoms are reported to be randomly occupied by vacancies for some type-I clathrate compounds such as K_8Ge_{44},[16,17] $(K,Cs)_8Sn_{44}$, and Rb_8Sn_{44}.[8] When judged from the weakness of x-ray intensities for superlattice reflections observed presently for Ba_8Ge_{43}, the intensities for superlattice reflections, if any, for these off-stoichiometric type-I clathrate compounds are expected to also be very weak. We thus cannot exclude the possibility where vacancies are distributed in an ordered manner also in these off-stoichiometric type-I clathrate compounds. In fact, a small amount of P vacancies in sites corresponding to the 6c sites of the type-I clathrate structure is recently reported to arrange in an ordered manner in an off-stoichiometric type-I clathrate compound $I_8Sn_{14}I_{10}P_{21.2}$ so as to form a tetragonal superstructure with the space group of $P4_2/m$.[21] As clearly demonstrated in the present study, electron diffraction is powerful to easily observe superlattice reflections arising from an ordered arrangement of vacancies and thus to identify the corresponding superlattice structure.

Type-I clathrate compounds K_8Ge_{44},[16,17] $(K,Cs)_8Sn_{44}$, and Rb_8Sn_{44},[8] in which vacancies are believed to randomly occupy one-third of the 6c sites, are of semiconductor that can be interpreted on the basis of the Zintl-Klemm concept,[22] since in the unit cell of these clathrate compounds, the number of the valence electrons of the guest atoms (1×8) is identical to that of the dangling bonds produced by two vacancies (4×2). On the other hand, there are four excess electrons per unit cell (when referring to the usual type-I clathrate structure) for Ba_8Ge_{43} because only 12 of 16 valence electrons of eight Ba atoms are compensated by three Ge vacancies. This indicates that Ba_8Ge_{43} may not be a semiconductor of the Zintl-Klemm concept. However, the temperature dependence of electrical resistivity for Ba_8Ge_{43} is of semiconductor [Fig. 10(a)]. The discrepancy may be ascribed to the change in the electronic structure due to the formation of the superstructure with the ordering arrangement of Ge vacancies in half the 6c sites of the usual type-I clathrate structure. The value of electrical resistivity of a disordered structure can be significantly different from that of the corresponding ordered structure for some intermetallic compounds such as CuPt (Ref. 23) since with the formation of the ordered structure, a Brillouin zone is produced inside the Brillouin zone of the disordered structure (Fig. 13).[24] Introduction of the zone tends to stabilize the ordered structure by the reduction of the total energy due to the readjustment of electron distribution, simultaneously modifying the Fermi surface.[25] If the excess electrons in the conduction band move to the valence band in order to readjust the electron distribution in Ba_8Ge_{43} on the formation of the superlattice structure, the Fermi surface falls to the energy band gap so as to exhibit a semiconducting behavior.

As a result, the thermoelectric properties of Ba_8Ge_{43} are not particularly good, as exemplified by the rather low ZT value of 0.057. For the property improvement of Ba_8Ge_{43},
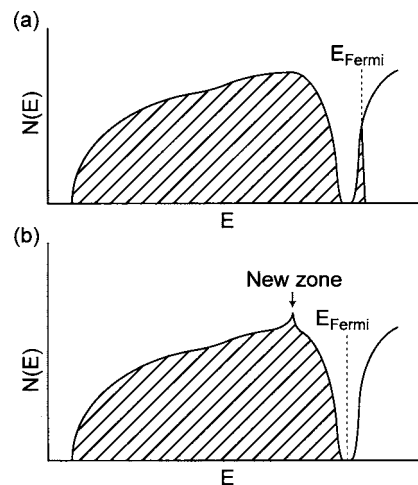

FIG. 13. Schematic illustrations of density-of-state curves for (a) disordered and (b) ordered structures.

some alloying elements such as Ga that preferentially occupies the Ge vacancy sites and restores the usual type-I structure may be effective. Investigation to deduce the relationships between the transport properties and the occupancy behavior for the 6c sites for $Ba_8Ga_XGe_{46-X}$ alloys at small levels of Ga additions is under way in our group.

V. CONCLUSIONS

(1) The crystal structure of Ba_8Ge_{43} is different from that reported for the usual type-I clathrate compounds with the space group of $Pm\bar{3}n$ but is a superlattice structure based on the usual type-I clathrate structure with the doubled lattice parameter. The superlattice structure is formed as a result of the ordering of Ge vacancies in half the 6c sites of the usual type-I clathrate structure. The crystal structure belongs to the space group of $Ia\bar{3}d$ and Ge vacancies exclusively occupy 24c sites.

(2) The value of electrical resistivity of Ba_8Ge_{43} is as high as 10^{-3} Ω m at room temperature, exhibiting the negative temperature dependence, which is typical of semiconductor. The semiconducting behavior of electrical resistivity is considered to originate from the formation of the superstructure due to the ordering of Ge vacancies. Because of the high electrical resistivity, the thermoelectric properties of Ba_8Ge_{43} are not particularly good, as exemplified by the rather low ZT value of 0.057.

ACKNOWLEDGMENTS

[1] *Hawley's Condensed Chemical Dictionary*, 14th ed., edited by R. J. Lewis (Wiley, New York, 2001), p. 274.

[2] J. S. Kasper, P. Hagenmuller, M. Pouchard, and C. Cros, Science **150**, 1713 (1965).

[3] C. Cros, M. Pouchard, P. Hagenmuller, and J. S. Kasper, Bull. Soc. Chim. Fr. **7**, 2737 (1968).

[4] C. Cros, M. Pouchard, and P. Hagenmuller, J. Solid State Chem. **2**, 570 (1970).

[5] J. Gallmeier, H. Schäfer, and A. Weiss, Z. Naturforsch. B **24**, 665 (1969).

[6] B. Eisenmann, H. Schäfer, and R. Zagler, J. Less-Common Met. **118**, 43 (1986).

[7] G. S. Nolas, D. G. Vanderveer, A. P. Wilkinson, and J. L. Cohn, J. Appl. Phys. **91**, 8970 (2002).

[8] J.-T. Zhao and J. D. Corbett, Inorg. Chem. **33**, 5721 (1994).

[9] S.-J. Kim, S. Hu, C. Uher, T. Hogan, B. Huang, J. D. Corbett, and M. G. Kanatzidis, J. Solid State Chem. **153**, 321 (2000).

[10] *International Tables for Crystallography: Space-Group Symmetry*, 4th ed., edited by T. Hahn (Kluwer, Boston, 1996), Vol. A.

[11] G. S. Nolas, Mater. Res. Soc. Symp. Proc. **545**, 435 (1999).

[12] G. A. Slack, in *CRC Handbook of Thermoelectrics*, edited by D. M. Rowe (CRC, Boca Raton, FL, 1995), p. 407.

[13] G. S. Nolas, J. L. Cohn, G. A. Slack, and S. B. Schujman, Appl. Phys. Lett. **73**, 178 (1998).

[14] Y. G. Zhang, P. L. Lee, G. S. Nolas, and A. P. Wilkinson, Appl. Phys. Lett. **80**, 2931 (2002).

[15] R. F. W. Herrmann, K. Tanigaki, T. Kawaguchi, S. Kuroshima, and O. Zhou, Phys. Rev. B **60**, 13245 (1999).

[16] H.-G. von Schnering, Nova Acta Leopold. **59**, 168 (1985).

[17] G. K. Ramachandran, P. F. McMillan, J. Dong, J. Gryko, and O. F. Sankey, Mater. Res. Soc. Symp. Proc. **626**, Z13.2.1 (2001).

[18] W. C. Cabrera, H. Borrmann, R. Michalak, and Y. Grin, http://pc176.ph.rhul.ac.uk/presentations/ba6ge25struc.pdf

[19] F. Izumi and T. Ikeda, Mater. Sci. Forum **321**, 198 (2000).

[20] *Handbook of Chemistry and Physics*, 82nd ed., edited by D. R. Lide (CRC, Boca Raton, FL, 2001).

[21] M. M. Shatruk, K. A. Kovnir, M. Lindsjö, I. A. Presniakov, L. A. Kloo, and A. V. Shevelkov, J. Solid State Chem. **161**, 233 (2001).

[22] E. Zintl, Angew. Chem. **52**, 1 (1939).

[23] W. Klemm, Proc. Chem. Soc., London **1958**, 329 (1958).

[24] M. Ichikawa, H. Iwasaki, and S. Endo, Jpn. J. Appl. Phys. **20**, 623 (1981).

[25] J. F. Nicholas, Proc. Phys. Soc., London, Sect. A **66**, 201 (1953).